

L. Pustina¹, F. Mastroddi¹, P. Della Vecchia² & G. Cerino³

¹Department of Mechanical and Aerospace Engineering, Sapienza University of Rome, Via Eudossiana 18, 00184 Rome, Italy

²Department of Industrial Engineering, University of Naples "Federico II", Via Claudio 21, 80125 Naples, Italy ³LEONARDO, Aircraft Division, Italy

Abstract

The aviation industry is increasingly focused on developing next-generation green aircraft to mitigate environmental impacts. This study addresses the limitations of traditional weight estimation methods (Class I & II) in the context of innovative aircraft designs, particularly focusing on the wing-box structure.

The conceptual design of three distinct aircraft configurations, a reference regional aircraft, a hybrid-electric aircraft, and a full-electric aircraft, utilizes HEAD (Hybrid-Electric Aircraft Design), an internally developed software at the University of Naples Federico II.

This study introduces a novel Class III weight estimation approach, developed at Sapienza University of Rome, integrating Finite Element Analysis (FEA) capabilities. This method facilitates rapid generation of detailed FEM models, crucial for Multidisciplinary Design Optimization (MDO) loops. Automated aeroelastostatic and buckling analyses are conducted to ensure structural integrity under varied flight conditions, while accurate modeling of composite materials like Carbon Fiber Reinforced Plastic (CFRP) enhances realistic weight predictions. Utilizing the developed Class III approach, this study optimizes the wing-box structure of the concepts developed.

oped with HEAD and emphasizes the differences in terms of structural weight.

Results demonstrate significant weight reductions in optimized wing-box structures while maintaining structural

integrity compared to the initial guess oversized FEM. Key optimization strategies include exploring design variables (e.g., ply thickness, spar cap width, stringer dimensions) using a genetic algorithm. Notably, tapering thickness along the wing-box's spanwise direction is crucial in achieving these weight reductions.

Comparison with HEAD software's structural mass estimations reveals good correlation for the wing-box, with differences noted in lighter (ICE and ICE+BAT) and heavier (PEMFC+BAT) configurations. Larger discrepancies are evident in unoptimized components like the fuselage and tail, highlighting areas for future refinement.

Keywords: Multi disciplinary optimization, Structural aircraft design, Conceptual and preliminary design

1. Introduction

The aviation industry faces an urgent challenge to mitigate greenhouse gas emissions and embrace sustainable practices. This pressing issue necessitates the development of next-generation green aircraft [1]. The Italian national project "MOST-Spoke 1 - AIR MOBILITY" is at the forefront of this endeavor, focusing on the design of green aircraft. As part of this project, the LEONARDO Company 1 provides a set of Top-Level Aircraft Requirements (TLARs), outlined in Table 1. The reference architecture is a conventional internal combustion engine (ICE) regional turboprop, representing a 2020 technology entry-into-service (EIS). The concept aircraft should be representative of a 2040 EIS configuration with comparable TLARs.

Parameter	Reference 2020	Concept 2040	
Number of passengers	48 (@30 inches)		
Design Payload (kg)	4560 (@95	5 kg/pax)	
Range @Design Payload (nm)	750	600	
Take-Off Field Length, ISA SL, @MTOW (m)	1200	1000	
Landing Field Length, ISA SL, @MLW (m)	1150	900	
Time to Climb, ISA, 200FL, @MTOW (min)	15	13	
Max speed, ISA 200FL, @97% MTOW (KTAS)	280	300	
One Engine Out Ceiling, ISA, @97% MTOW (ft)	>14000	>15000	
EIS	-	2040	

Table 1 - Aircraft TLARs

Based on the TLARs provided in Table 1, the conceptual design is carried out using the University of Naples Federico II's internally developed software, HEAD (Hybrid-Electric Aircraft Design). This software, written in MATLAB, can handle both conventional and unconventional powertrain architectures [2, 3]. The main structural empty weight (EW) masses are estimated using conventional aircraft design statistical regressions as suggested by Torenbeek [4]. To accurately assess the effects of new technologies, several reduced order models (ROM) are integrated into HEAD. These include models for wing structural masses in high aspect ratio and distributed propulsion configurations, as well as hydrogen tank masses.

The aviation industry must address several challenges when applying this approach to innovative green aircraft. The introduction of new concentrated masses, such as batteries and fuel cells, significantly impacts loads and requires careful design considerations to ensure that the aircraft structures can accommodate these components while maintaining optimal performance and structural integrity. The shift to electric power sources, like batteries or fuel cells, enables the adoption of innovative propulsion systems such as distributed electric propulsion. These systems can significantly influence both loads and structural weight, rendering traditional empirical predictions less reliable. Additionally, the integration of advanced materials, such as Carbon Fiber Reinforced Plastic (CFRP), leads to substantial reductions in structural weight, challenging the accuracy of traditional empirical predictions for structural-weight estimates.

Groundbreaking design solutions, like truss-braced wings, folding wing tips for high aspect ratio wings, and blended wing body configurations, further highlight the inadequacy of relying on traditional empirical predictions. These advanced designs demand new methodologies to capture the complex dynamics and weight distribution associated with innovative aircraft.

Weight estimation methods in aircraft design are categorized into several classes:

- Class I: Used in early conceptual phases to estimate Maximum Take-off Weight (MTOW), Operational Empty Weight (OEW), Payload Weight (PLW), and Fuel Weight (FW) based on statistical data and basic performance equations [5, 6, 4].
- Class II: Used when baseline geometry is established, employing semi-empirical relations to estimate component weights [5, 4, 7].

¹LEONARDO Company Website: https://www.leonardo.com. Accessed 12/01/2024

- Class III: Uses physics-based Finite Element Analysis (FEA) for detailed component sizing and weight estimation [8, 9, 10].
- Class IV: Applied during detailed and pre-production phases, combining advanced FEM models with production CAD models and actual component weights from catalogs and suppliers.

Class I and II methods are useful in preliminary design but face challenges with innovative aircraft designs. New concentrated masses (e.g., batteries, fuel cells) and advanced materials (e.g., CFRP) require detailed design considerations to ensure structural integrity and optimal performance.

In this study, we introduce an advanced Class III weight estimation approach. This method rapidly generates a Finite Element Method (FEM) model for the entire aircraft in less than a minute, facilitating integration into a Multidisciplinary Design Optimization (MDO) loop. The software supports automated aeroelastostatic and buckling analyses, and models composite structures, including sandwich components. This Class III approach has been applied in the open-loop analysis of a hybrid regional aircraft by the authors [11].

In this study, the conceptual design strategy is first described in Section 2. Next, the developed Class III weight estimator and the wing-box structural optimization approach are detailed in Section 3. The proposed design approach is then employed to develop two distinct innovative green aircraft concepts: a hybrid-electric aircraft powered by Li-ion batteries and ICE, and a full-electric configuration featuring fuel cells and Li-S batteries. Additionally, a reference traditional regional aircraft is designed using the same methodology. Finally, Section 4.discusses the numerical results, including the main aircraft parameters from the conceptual design process and the structural response for the different concepts.

2. Description of the Conceptual Design Strategy

Based on TLARs provided in Table 1, the conceptual design has been performed through the University of Naples Federico II internally developed software called HEAD (Hybrid-Electric Aircraft Design), written in MATLAB language, capable to handle both conventional and unconventional powertrain architectures (see [2][3]). HEAD software is based on a simulation-based approach conceived to perform design and mission simulation of propeller-driven architecture characterized by conventional or unconventional powertrain with serial, parallel, serial-parallel architecture, distributed electric propulsion, handling at the same time up to 3 different sources of energy from conventional fuel, batteries or fuel cells. Starting from typical point-sizing approach based on the requirements, HEAD firstly performs a initial sizing accordingly an energetic method [2] and then refine iteratively the design by doing a point mass mission simulation [3]. The final architecture is represented by a data structure containing information on geometry, masses, aerodynamic and performance (included noise and emissions).

The main innovation of HEAD is the ability to deal with complex propulsive architectures, including more than one propulsion source and distributed electric propulsion. The main impact of these technologies compared to conventional aircraft is given by the different chain of efficiencies and, above all, by the non-negligible associated mass penalty. The main structural empty weight masses (EW) are estimated through conventional aircraft design statistical regressions as suggested by Torenbeek [4]. In order to correctly grasp the effects of these technologies, modelling both their advantages and disadvantages, several reduced order models (ROM) are integrated in HEAD, such as the wing structural masses for high aspect ratio and distributed propulsion and the hydrogen tank masses.

The HEAD overall workflow is depicted in Fig.1. For a given aircraft geometrical configuration and mission profile specifications, the weight loop estimation carefully account for structural masses, powertrain masses and energy sources masses. Subsequently, the mission simulation and performance analysis computes the ground, flight and mission profile performance with a simulation based approach. Performing detailed simulation-based mission analysis is essential for estimating the impact of hybrid-electric propulsion on aircraft flight mission parameters. Such analysis requires characterizing each step of the entire flight mission by its aerodynamic and propulsive features. Consequently, all aspects defining the aircraft's state at each step—such as Mach number, altitude, throttle setting, acceleration, and rate of climb—must be determined to simulate the flight history accurately. In the HEAD approach, flight simulation is utilized to evaluate the effects of masses and efficiencies across various design phases. This includes integrating weight estimation models that account for masses not typically considered in the aircraft pre-design phase. At each time step, the following activities are performed: (i) Starting from the flight conditions at the beginning of the flight segment, the aerodynamic characteristics are computed. (ii) At the prescribed airspeed and altitude, the power distribution along the propulsion system is determined. (iii) With the aerodynamic and propulsive forces calculated, the new flight conditions are determined. The sequence of these phases varies depending on the flight segment. Notably, in cases involving aero-propulsive interactions, the first and second steps are linked in an iterative process. The HEAD powertrain module is capable to handle conventional, serial, parallel and serial/parallel powertrain architectures up to three different energy sources at the same time. A simplistic representation of the hybrid series/parallel electric powertrain is given in Fig. 2. The presented diagram refers to the case of two energy sources, where the thermal power source is marked as primary and the electric energy storage as a secondary source.

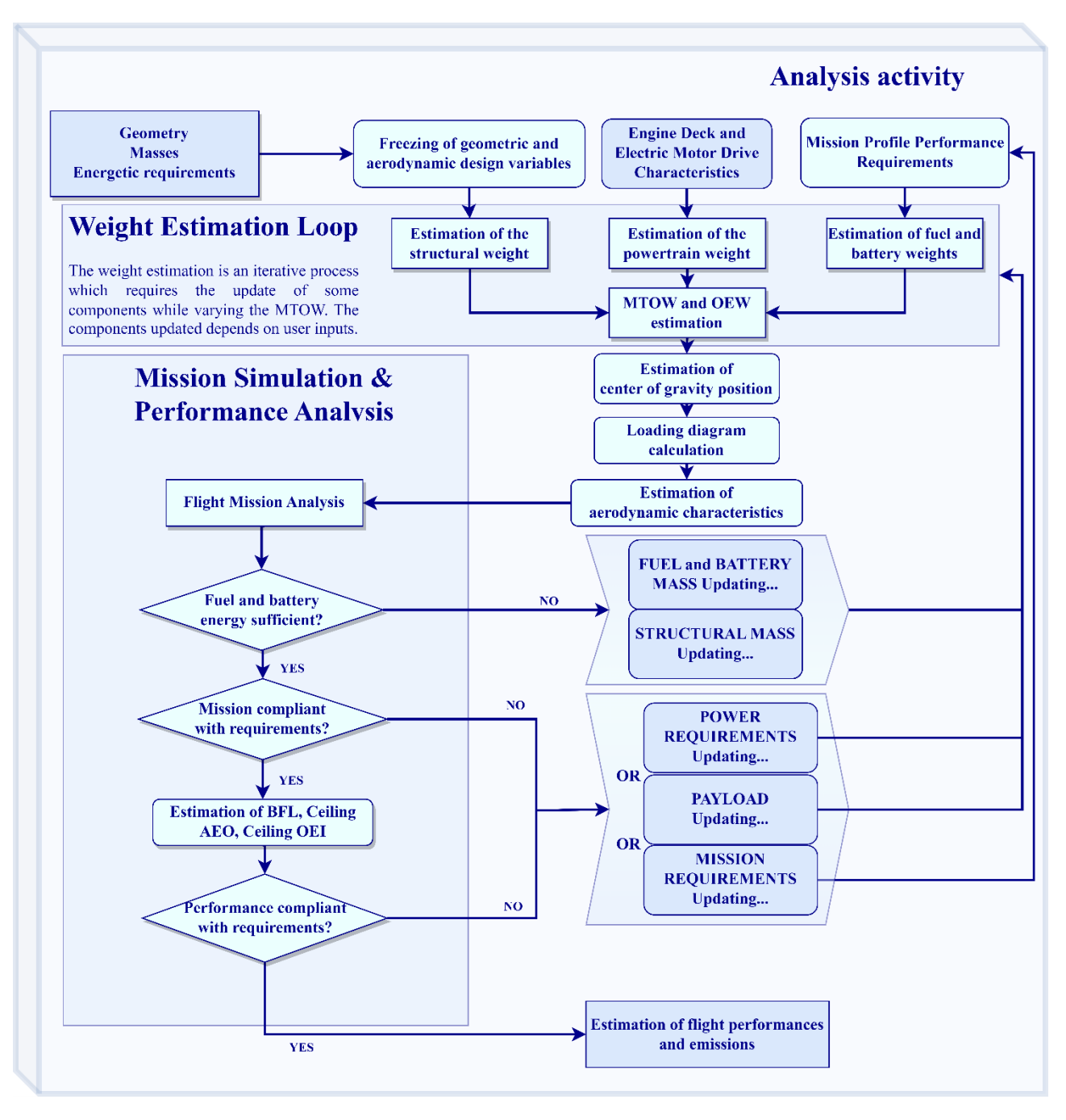


Figure 1 - Workflow of the analysis module of HEAD

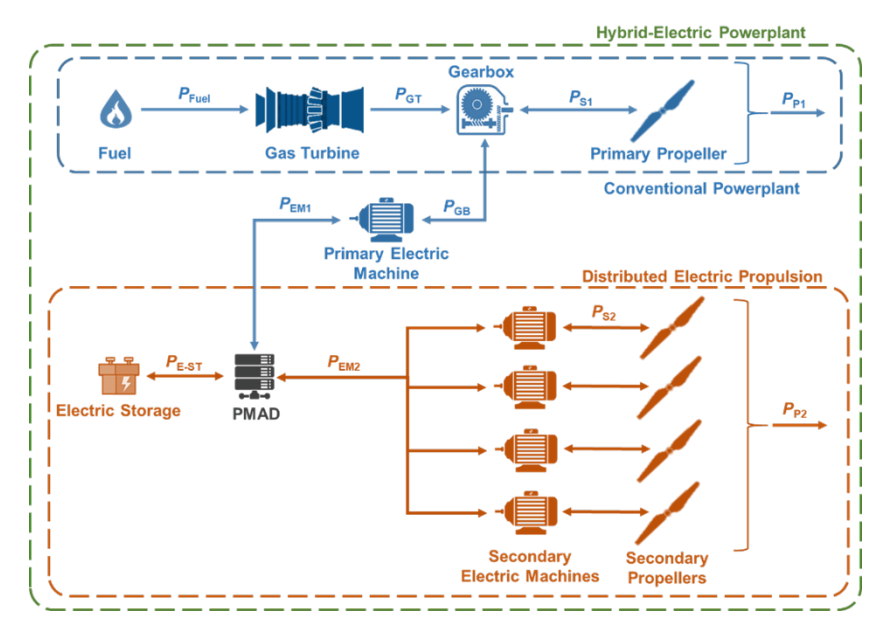


Figure 2 – Example of a hybrid-electric propulsive scheme

3. Description of the Wing-box Structural Optimization

This study addresses the limitations of Class I and Class II weight estimation approaches by developing an innovative, physics-based Finite Element Analysis (FEA) for a more detailed examination of aircraft structural components. This method is particularly suited for specific concentrated mass distributions, such as batteries or distributed electric propulsion systems, and supports the modeling of composite structures, such as CFRP.

An automated optimization process was created, utilizing a simplified finite element model (FEM) of the entire aircraft. The objective of this optimization is to minimize structural mass while maintaining structural integrity. The design variables include not only the thickness of various structural components (such as skin, spar webs, and spar caps) but also geometric parameters of structural elements, like the width of spar caps, which necessitate complete FEM regeneration and remeshing. A complete list of the design variables and their relative bounding boxes is provided in Section 4.2 The optimization process starts with the utilization of the in-house FUROR code (Framework for Automatic Generation of Aeroelastic Models), preliminary results obtained using this framework were presented at the AIDAA conference [11]. This code employs structural and geometric design variables to generate a simplified Computer-Aided Design (CAD) model of the entire aircraft using the opensource library OpenCasCADE. This comprehensive model encompasses various structural components, including (but not limited to) spar web and wing ribs. The components are then meshed using the open-source code Gmsh (Ref. [12]), adopting a hybrid structured/unstructured meshing strategy. To estimate aerodynamic loads, aerodynamic surfaces modeled with the doublet lattice method are embedded within the Nastran model. A precise structural weight estimation is performed on the Nastran FEM model, providing a robust and reliable assessment. Subsequently, the non-structural masses of the propulsion system and the payload, arising from the previous design phase, are accurately positioned within the model. Next, an aeroelastic static analysis is conducted using Nastran sol144 [13], considering the most critical flight envelope conditions to determine the static aeroelastic loads acting on the aircraft and assess its structural integrity. Furthermore, the aerodynamic loads obtained from sol144 are applied to perform a linear buckling analysis (sol105 [14]) to verify the stability and robustness of the structural design.

The developed approach is applied to three different configuration outputs from the conceptual design (see Section 4.). Numerical results, including weight comparison with Class I and II approaches and structural response, are described in Section 4.2

4. Numerical Results

Numerical results will be presented, highlighting the critical aspects of the optimized structures for the three configurations: traditional, hybrid batteries, and hybrid hydrogen. These results will also include comparisons of the resulting structural masses to those achieved using the conventional statistical estimation based on historical trends.

4.1 Conceptual Design

The results of the conceptual design of an entry into service (EIS) scenario 20240 are provided in this section. Firstly the reference EIS was set to 2040 for this scenario: a conventional airplane defined for a 2040 EIS. subsequently a hybrid-electric airplane with ICE and Li-S/SSB batteries designed for the same EIS target is presented. Finally, an aeroplane concept with PEMFC and Li-S/SSB batteries is presented. The aeroplane model similar to an ATR 72-600 designed with HEAD (with an EIS 2020) was used as a baseline for the definition of all three aeroplanes [1]. For a fair comparison, the same assumptions were adopted for those technologies applied on more than one concept model, i.e., the same level of technology and overall-pressure-ratio (OPR) for the gas turbine engines installed on the conventional and on the hybrid-electric airplane with ICE, same specific power and efficiency for the Li-S and SSB batteries installed on the hybrid-electric concepts with ICE and PEMFC. Table 2 shows the considered enabling technologies during the conceptual design phase.

Table 2 - Enabling Technologies summary table.

Technology Description	Power	Mass	Specific Power	Efficiency	RPM
	kW	kg	$kWkg^{-1}$	%	rev/min
Liquid-cooled PMSM with hairpin windings	290	53.5	5.42	95	8000
PMSM with Halbach array and directly cooled stator windings	1700	154.9	10.98	95	4000

-		
Converter	Efficiency	Power Density
Motor drive inverter	99.0%	$63 \mathrm{kW kg^{-1}}$
Generator drive inverter	99.0%	$63\mathrm{kWkg^{-1}}$
Battery DC/DC converter	98.0%	$50\mathrm{kWkg^{-1}}$
Fuel cell DC/DC converter	98.0%	$50 \mathrm{kW kg^{-1}}$
Parameter	Li-S	SSBs
System-specific energy $(Wh kg^{-1})$	675	585
Nominal C-rate (1/h)	1.5	4.0
System energy density (WhL^{-1})	735	1001
Parameter	PEMFC	SOFC
System's gravimetric Power density $(Whkg^{-1})$	1.2	1.125
System's volumetric power density (WhL^{-1})	0.8	1.0
Hydrogen tank external di- ameter 1.0 m	Design Pressure 70MPa	



Figure 3 – Reference (left), hybrid concept 2040 (middle), full-electric concept 2040 (right)

4.1.1 Reference Aircraft

The design and analysis framework provided by HEAD was used to develop the reference airplane for the medium-term. The main objective was to try to match as close as possible the ATR 42-600 publicly available information on design weights, performance indicators (takeoff field length, landing field length, time-to-climb, ceiling, flight speeds), fuel consumption, and emissions characteristics. The design mission profile is the 726M standard ATR mission, with 48 passengers at 95kg each, including the the typical fuel reserves. The total fuel required by the mission is evaluated through an iterative loop on MTOW; the loop stops when MTOW variations are under a selected tolerance. Starting from the baseline model a new airplane with a conventional powerplant architecture featuring an internal combustion engine (ICE) as the sole source of propulsive power was designed. Compared to the baseline aircraft, new engines specifically designed for a 2040 entry into service (EIS) were created for this conventional airplane. The geometry of the baseline aircraft model remained unchanged, meaning the medium-term conventional airplane retains its original design characteristics, even though literature shows that innovative tailplane and fuselage tail-cone allow a structural weight and drag reduction [15]. This sub-section provides detailed information on design weights, powerplant characteristics, performance, and emissions of this concept vehicle. The design fuel (conventional kerosene) accounted for includes fuel used in all mission phases except taxi out, reserves for potential diversions, and an additional 5% reserve not consumed during the mission. The advantage in fuel burn and emissions of the advanced conventional aircraft is measured by evaluating several typical missions characterized by a shorter range; these calculations illustrate how fuel consumption and emission increase with decreasing mission ranges due to the shrinking impact of the cruise segment over the entire mission.

The aircraft mass breakdown shows that the weight reduction is related to the new engine characteristics. Table 3 collects the most relevant powertrain characteristics. A significant weight reduction can be observed when compared to the engines of the baseline model (see tables 4 and 5). Table 6 illustrates the main performance characteristics of the reference aircraft, compared with the TLAR set. The conventional aircraft concept matches all the main TLARs successfully. The analysis considered two different types of fuels.

Table 3 – Reference configuration powerplant characteristics.

Component	Quantity	Rated Power (kW)
Thermal Engine	2	1589 (x2)
Parameter	Value	Unit
Rated Power	1589	kW
Specific Fuel Consumption	0.2294	$kg(kWh)^{-1}$

Table 4 – Reference configuration Operating Empty Mass.

Component	Value	Unit
Wing	1484.1	kg
Horiz. Tail	201.0	kg
Vert. Tail	257.4	kg
Fuselage	2374.3	kg
Control surfaces	329.9	kg
	645.9	•
Main Undercarriage	151.3	kg
Nose Undercarriage		kg
Primary Nacelles	377.1	kg •
Total Structural Weight	5821.2	kg
Fuel Systems (Thermal)	114.7	kg
Thermal Engines		
(including primary	505.6	kg
gearboxes)		
Primary propellers	657.2	kg
Total Powerplant Weight	1277.9	kg
Air conditioning	591.4	kg
Electrical systems	741.6	kg
Pneumatic/Hydraulic Systems	412.2	kg
Instruments	321.9	kg
APU	181.6	kg
Total Systems Weight	2248.8	kg
Furnishing	1158.8	kg
Total Furnishing Weight	1158.8	kg
Crew	380.0	kg
Operational items	430.9	kg
Operative Equipment Weight	810.9	kg
Operating Empty Mass	11317.6	kg
- h		9

Table 5 – Mass breakdown for the reference configuration.

Component	Value	Unit
Structure	5821.2	kg
Powerplant	1277.9	kg
System	2248.8	kg
Manufacturer Empty Mass	9347,9	kg
Furnishing	1158.8	kg
Empty Mass	10506.7	kg
Operative Equipment	810.8	kg
Operating Empty Mass	11317.6	kg
Design Payload	4750.0	kg
Zero Fuel Mass	16067.6	kg
Maximum Payload	4750.0	kg
Maximum Zero Fuel Mass	1353.7	kg
Maximum Takeoff Mass	17421.3	kg

Table 6 – Reference aircraft main performance and energy/fuel consumptions.

Parameter	Unit	Va	TLAR	
		Kerosene	HEFA-SPK	
Design range	nmi	600	600	600
Typical range	nmi	200	200	200
MTOW	kg	17421	17398	< 24000
Service Ceiling (AEO)	ft	21005	21005	< ∞
Service Ceiling (OEI)	ft	11522	11522	< ∞
Time to Climb	min	12.59	12.59	< 13.0
Takeoff Distance	m	723	723	< ∞
Takeoff BFL	m	989	989	< 1200
Landing Distance	m	712	712	< ∞
Landing Field Length	m	1187	1187	< 1200

4.1.2 Hybrid Electric Aircraft

The Hybrid-Electric Configuration, starting from the enabling technologies illustrated in Table 7, adopts a Thermal engine coupled with distributed propulsion electric engines supplied by batteries. The wing is a fully composite material (carbon/epoxy-based) structure; the overall wing surface is $59.10\,\mathrm{m}^2$, with a wingspan of $26.96\,\mathrm{m}$. Table 8 illustrates the selected geometrical properties for this design. The ICEs can use kerosene or SAF.

The DOE approach was based on the aircraft having the minimum block fuel, matching all the TLARs; the best hybridization factors for each mission segment (taxi on the ground, takeoff, climb, cruise, loiting/orbiting, landing) were researched through an iterative process considering the effect of design variables on aircraft masses, aerodynamics parameters and final performance figures of merit. This analysis included 1500 possible Hybrid-Electric architectures based on already-in-service aircraft to reduce design and production costs, enabling the EIS in less than ten years. The main objective was to preserve the baseline aircraft geometry and structural weight, including the undercarriage. The optimal battery mass is the one that guarantees the best compromise between available electric energy and the energy necessary for the accomplishment of the design mission.

The final MTOW of the configuration is more than 6 tons higher than the conventional reference aircraft, with 23021.0 kg. Table 9 shows the overall mass breakdown of the configuration, while Table 10 illustrates the mass balance.

Table 7 – Technological scenario for the Hybrid-Electric configuration.

Technology	Туре
Scenario Identifier	EIS 2040: ICE + Battery
Wing structure material	Carbon/Epoxy (AS4/3501-6)
Secondary Power Source	Liquid Cooled PMSM and PMSM with
	Halbach Array and Direct Cooled Stator
	Windings + Li-S Batteries or SSB
Power Electronics	SiC Converters

Table 8 – Hybrid-Electric configuration geometrical characteristics.

Parameter	Value	Unit
	Wing	
Surface	59.10	m^2
Span	26.96	m
Aspect Ratio	12.30	Non dimensional
Root chord	2.56	m
Tip chord	1.38	m
Hori	zontal ta	nil
Surface	11.03	m^2
Span	7.25	m
Aspect Ratio	4.77	Non dimensional
Root chord	1.92	m
Tip chord	1.12	m
Ver	tical tail	
Surface	14.72	m^2
Span	4.93	m
Aspect Ratio	1.65	Non dimensional
Root chord	3.66	m
Tip chord	2.32	m
Fı	ıselage	
Total length	22.67	m
Reference diameter	2.87	m

Table 9 – Hybrid-Electric Mass breakdown.

Value	Unit
6495.1	kg
6084.4	kg
2676.1	kg
15255.7	kg
1158.8	kg
16414.5	kg
810.9	kg
17225.3	kg
4750.0	kg
21975.3	kg
4750.0	kg
21975.3	kg
1045.7	kg
23021.0	kg
	6495.1 6084.4 2676.1 15255.7 1158.8 16414.5 810.9 17225.3 4750.0 21975.3 4750.0 21975.3

Table 10 – Hybrid-Electric configuration balance.

Balance		Center of Gravity				
Item	Value	Unit	$X_{c.g.}$	$Y_{c.g.}$	$Z_{c.g.}$	Unit
Structure	6495.1	kg	10.333	0.000	0.795	m
Powerplant	6084.4	kg	9.326	0.000	0.660	m
System	2676.1	kg	8.939	0.000	0.513	m
Furnishing	1158.8	kg	9.240	0.000	0.000	m
Operative Equipment	810.9	kg	8.125	0.000	0.000	m
Design Payload	4750.0	kg	9.240	0.000	0.000	m
Design Fuel	1045.7	kg	9.969	0.000	0.000	m
MTOM	23021.0	kg	9.530	0.000	0.079	m
	X	$K_{c.g.} =$	25 % M.A	A.C.		

The powertrain is a serial/parallel partial hybrid architecture, with 2 ICE and 8 distributed electric propulsion engines (DEP configuration), with two distinct propulsive lines, enhancing safety and fault tolerances considerations [3]. Gearboxes automatically control the propeller nominal RPMs, with the electrical machines' RPMs equal to 8000. Gearboxes automatically control the propeller nominal RPMs, with the electrical machines' RPMs equal to 8000. The DEP increase the lifting capabilities during the takeoff phase, compensating for the greater MTOW of this configuration; during cruise phases, however, the best power management is achieved directing all the power to the primary shafts. Complexities related to aircraft handling qualities, controllability and behaviour in the presence of a fault or damage are not considered in this work [16]. Power and energy requirements drive the selection of Li-S batteries as the best design choice for this powertrain, with half of the total power located in each wing [17]. This assumption made it possible to complete a typical mission of a shorter length concerning the design mission by working almost entirely with the battery, even during the cruise phase. However, it is anticipated that the typical mission described discharges the battery to only 50%, which allows shorter recharging times and more flights of the same vehicle per day. Table 12 shows the Hybrid-Electric performances and energy/fuel consumption.

The design mission profile is a $600\,\mathrm{M}$ flight, while a typical mission profile is a $200\,\mathrm{M}$ flight. At the end of the mission energy is not completely depleted, since a $5\,\%$ fuel reserve and a battery charge not less than $20\,\%$ are still available. Table 12 shows performance data, also comparing results using standard kerosene and HEFA - SPK sustainable aviation fuel (SAF).

Table 11 – Main powertrain components for the Hybrid - Electric configuration.

Component	Quantity	Rated Power (kW)
Thermal engines	2	1009 (x2)
Primary Electrical Machines	2	1700
Secondary Electrical Machines	8	290 (x8)
Battery	2	1670 (x2)
Item	Value	Unit
Rated Power	1009	kW
Operative Equipment	0.2402	$kg\;(kW\;h)^{-1}$

Table 12 – Hybrid-Electric aircraft main performance and energy/fuel consumptions.

Parameter	Unit	Va	TLAR	
		Kerosene	HEFA-SPK	
Design range	nmi	600	600	600
Typical range	nmi	200	200	200
MTOW	kg	23040	23021	< 27000
Service Ceiling (AEO)	ft	23126	23126	< ∞
Service Ceiling (OEI)	ft	12674	12674	< ∞
Time to Climb	min	12.68	12.68	< 13.0
Takeoff Distance	m	798	798	< ∞
Takeoff BFL	m	920	920	< 1200
Landing Distance	m	702	702	< ∞
Landing Field Length	m	1170	1170	< 1200

4.1.3 Full-Electric Aircraft

The Full-Electric Configuration is again designed by choosing the aircraft with minimum block fuel, satisfying all the TLARs provided. The powertrain architecture is based on a fuel cell system, where electricity is produced by the fuel cells through the reaction of hydrogen with air; atmospheric air is supplied through suitable air intakes and compressed up to the operating pressure using a centrifugal compressor; impact of air intakes which are necessary for the operation of fuel cells on the aircraft mass and aerodynamics was neglected. Tables 16 and 17 illustrate the Full-Electric configuration mass breakdown and balance.

A single propulsion line with ten electric motors supplies the required thrust with a beneficial decrease in production and maintenance costs because all the installed electric motors are rated at the same power. The MTOW of this configuration is about 9 tons higher than the conventional architecture. Table 13 illustrates the Full-Electric configuration technological scenario.

Based on the power and energy requirements, Li-S batteries were identified as the best choice for this application. The aircraft is characterized by a single propulsive line with ten electric motors, expected to benefit production and maintenance costs. Table 15 illustrates the Full-Electric aircraft powertrain main characteristics. The value of battery power reflects the total power provided by the batteries installed on the airplane; half of this power should be considered per wing (1828kW); this analysis do not take into account batteries used as load-carrying structural elements [17]. The selected rotational speed for the electric engines is $4000\,\mathrm{RPM}$ with reduction gearboxes to adapt propeller rotation speed.

Table 13 – Technological scenario for the Full-Electric configuration.

Technology	Туре					
Scenario Identifier	EIS 2040: PEMFC + Battery					
Wing structure material	Carbon/Epoxy (AS4/3501-6)					
Fuel Cells	Proton Exchange Membrane Fuel Cells					
Batteries	Li-S Batteries or SSBs					
Electric Machines	PMSM with Halbach Array and Direct					
	Cooled Stator Windings					
Power Electronics	SiC Converters					
Fuel	Hydrogen					
Fuel Tanks	Pressurized Hydrogen Tanks					

Table 14 – Full-Electric configuration geometrical characteristics.

Parameter	Value	Unit				
	Wing					
Surface	70.18	m^2				
Span	30.25	m				
Aspect Ratio	12.93	Non dimensional				
Root chord	2.73	m				
Tip chord	1.47	m				
Hori	zontal ta					
Surface	12.30	m^2				
Span	7.65	m				
Aspect Ratio	4.77	Non dimensional				
Root chord	2.03	m				
Tip chord	1.19	m				
Ver	tical tail					
Surface	17.11	m^2				
Span	5.31	m				
Aspect Ratio	1.65	Non dimensional				
Root chord	3.66	m				
Tip chord	2.50	m				
Fuselage						
Total length	26.40	m				
Reference diameter	2.87	m				

Table 15 – Full-Electric main powertrain components.

Component	Quantity	Rated power kW
Fuel Cell System	2	1180 (×2)
Electric Machines	10	600 (×10)
Battery	2	1828 (×2)

Table 16 – Full-Electric Mass breakdown.

Component	Value	Unit
Structure	7756.5	kg
Powerplant	10835.7	kg
System	3080.1	kg
Manufacturer Empty Mass	21672.4	kg
Furnishing	1290.8	kg
Empty Mass	22963.2	kg
Operative Equipment	810.9	kg
Operating Empty Mass	23774.0	kg
Design Payload	4750.0	kg
Zero Fuel Mass	28524.0	kg
Maximum Payload	4750.0	kg
Maximum Zero Fuel Mass	28524.0	kg
Design Fuel	390.7	kg
Maximum Takeoff Mass	28914.7	kg

Table 17 – Full-Electric configuration balance.

Balanc	Center of Gravity					
Item	Value	Unit	$X_{c.g.}$	$Y_{c.g.}$	$Z_{c.g.}$	Unit
Structure	7756.5	kg	12.133	0.000	0.704	m
Powerplant	10835.7	kg	10.792	0.000	0.572	m
System	3080.1	kg	10.286	0.000	0.503	m
Furnishing	1290.8	kg	10.382	0.000	0.000	m
Operative Equipment	810.9	kg	8.978	0.000	0.000	m
Design Payload	4750.0	kg	10.760	0.000	0.000	m
Design H2	390.7	kg	11.609	0.000	1.433	m
MTOM	28914.7	kg	11.034	0.000	0.066	m
	$\mathbf{X}_{c.g.} =$		25 % M.A	A.C.		

Table 14 illustrates the Full-Electric geometrical characteristics. Wing span and surface are greater than the Hybrid-Electric configuration.

Table 18 – Main characteristics for the aircraft configurations under development.

Parameter		Unit	Reference	е		Concept		
Aircraft Powertrain			Baseline	EIS 2040 ICE	Hybrid 2040 ICE		Full- electric20 PEMFC	040
Entry Into Service Primary Fuel Primary Power		year - -	Value 2020 Kerosene	2040 Kerosene ICE	+ Battery Value 2040 HEFA- SPK ICE	Diff.	+ Battery Value 2040 Pressuriz H2 PEMFC	Diff.
Source Secondary Power		-	-	-	Li-lon		Li-S	
Source Design Range		nmi	750	600	Battery 600	- 17.40%	Battery 600	- 17.40%
Cruise Altitude		ft	24000	24000	20000	- 16.70%	20000	- 16.70%
Maximum Take-Off Mass		kg	18627	17421.3	23021	55.20%	28915	55.20%
		6	00 nmi Des	ign Missio	n			
Fuel/H2	Block	kg	1481.5	1003.92	730	- 50.70%	229.6	- 84.50%
	Total	kg	1982	1345.91	1033.7	- 47.80%	317.5	- 84.00%
Fuel/H2 Energy	Block	MWh	17.78	12063.8	8.93	- 49.80%	7.65	- 57.00%
	Total	MWh	23.78	16173.4		- 46.80%	10.58	- 55.50%
Battery Energy	Block Total	MWh MWh	0	-	1.8	100.00% 100.00%	1.95	100.00% 100.00%
CO2	Block	kg	4665.1	3161.344	2263	- 51.50%	0	100.00%
	Total	kg	6241.3	4238.260	3204.4	- 48.70%	0	100.00%
NOx	Block	kg	17.91	12.077	10.05	43.90%	0	100.00%
	Total	kg	20.88	14.995	13.4	35.90%	0	100.00%
H2O	Block	kg	1822.2	1234.822	987.7	- 45.80%	2051.8	12.60%
	Total	kg	2437.8	1655.465	1398.6	- 42.60%	2838	16.40%
		2	00 nmi Typi	cal Missio	n			
Fuel/H2	Block	kg	610.7	431.54	237.1	- 61.20%	61.8	- 89.90%
	Total	kg	1110	773.41	540.6	- 51.30%	149.7	- 86.50%
Fuel/H2 Energy	Block	MWh	7.33	5185.7	2.9	- 60.40%	2.06	- 71.90%
	Total	MWh	13.32	9293.8	6.61	- 50.30%	4.99	- 62.50%
Battery Energy	Block	MWh	0	-	0.9	100.00%		100.00%
CO2	Total Block	MWh kg	0 1923.2	- 1358.911	0.9 735	100.00%	0.97 0	100.00%
- +-	Total	kg	3495.4	2435.465		61.80%	0	100.00%
NOx	Block	kg	6.14	4.671	1.65	52.10% -	0	100.00%
	Total	kg	9.1	7.587	4.99	73.10% -	0	100.00%
						45.20%		100.00%
H2O	Block	kg	751.2	530.791	320.8	- 57.30%	552.8	- 26.40%

4.2 Wing-box Structural Optimization

The second design phase presented in this work focuses on the structural optimization of the three configuration outputs from the conceptual design phase. A complete simplified aircraft FEM model is generated using the in-house FUROR software (see Section 3, incorporating all non-structural masses provided by the conceptual design to achieve accurate inertial properties. The mass breakdown of the reference FEMs for the three configurations is described in Section 4.1 The non-structural masses in the fuselage are connected to the fuselage frames using Nastran RBE3 elements [14]. This study does not focus on a detailed structural analysis of the fuselage; therefore, a simplified approach is adopted for positioning the non-structural masses. These masses are divided into three categories: nose masses, center fuselage masses, and fuselage tail masses. Each category is equally subdivided among the fuselage frames and linked using RBE3 elements. For a detailed mass breakdown for each configuration, refer to Section 4.1

Conversely, a more detailed approach is taken for the wing-box. For the Distributed Electric Propulsion cases (ICE+BAT and PEMF+BAT), special care is needed for positioning the non-structural masses. Specifically, two ribs are defined for each engine, and an RBE3 element is used to connect the engine to these ribs. Figure 4 shows the ribs and the concentrated engine masses considered for the analysis.

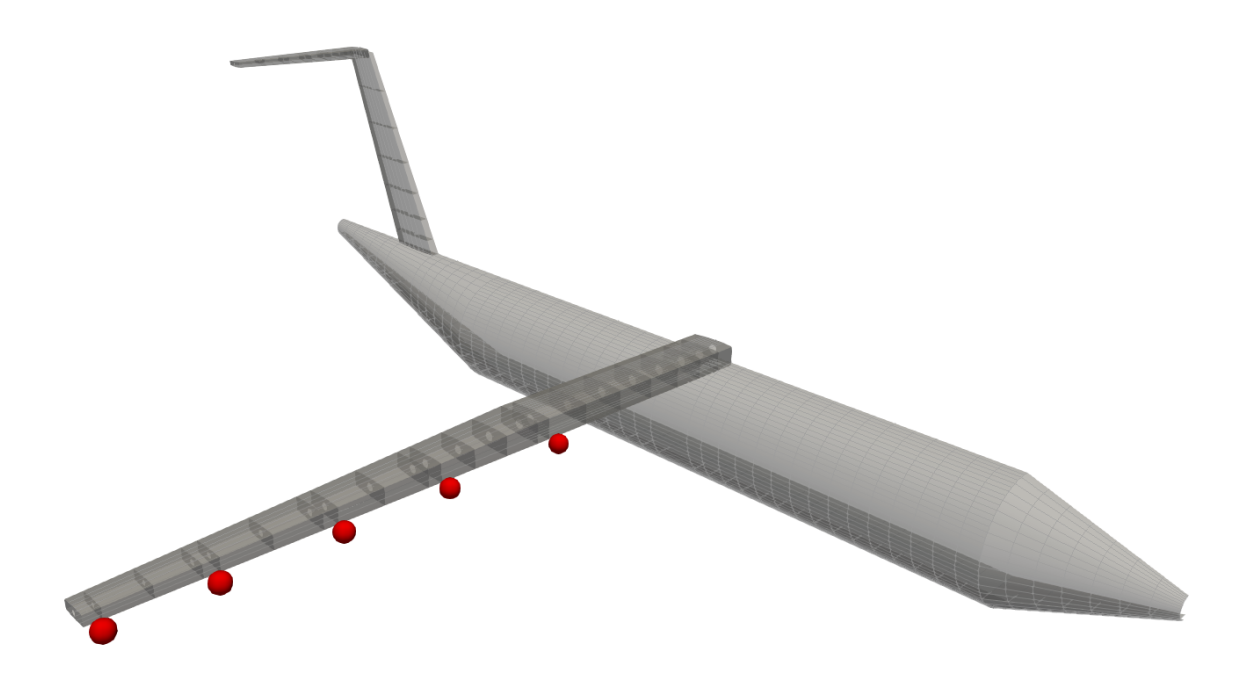


Figure 4 – Distribution of ribs and engine concentrated masses. The engine concentrated masses are depicted in red.

The rotor thrust and aerodynamic drag were neglected in this analysis, while the engine inertial load was properly distributed by the added ribs on the structure. Fuel and other non-structural masses of the wing were equally distributed among the wing ribs. Two different load factors were considered for the analyses: a positive limit load factor of 2.72 g (corresponding to a vertical gust of 50 ft/s at the maximum cruise speed of 267.3 knots) and a negative limit load factor of -1.0 g at the maximum cruise speed. These load factors were multiplied by 1.5 to achieve the ultimate loads used in the analysis, which are 4.08 g and -1.5 g, respectively (see Table 19).

Speed [knots]	Vertical Gust [ft/s]	Limit Load Factor [g]	Ultimate Load Factor [g]
267.3	50	2.72	4.08
267.3	-	-1.0	-1.5

Table 19 - Considered load cases.

After defining the non-structural masses and load cases, the first step in the optimization process was the creation of an initial guess configuration. Based on simple analytical beam models and preliminary FEM analyses, the authors designed a preliminary aircraft for each configuration (ICE, ICE+BAT, and PEMFC+BAT) by assigning thicknesses to all structural components. These initial configurations meet the structural integrity requirements but are oversized, allowing the optimizer to reduce the structural mass. Table 22 presents a comparison of the structural weights across different configurations. The table includes the structural masses estimated with HEAD (see Section 4.) and the structural masses estimated with the FEM for comparison.

After defining the initial Finite Element Models (FEMs) for the three configurations, the wing-box structures were optimized. To save computational time, the fuselage was excluded from structural optimization and treated as rigid within the optimization loop. However, the rudder and tail were included as elastic bodies in the optimization loop without their structures being optimized.

The objective function of the optimization is the wing-box structural mass, with constraints to ensure structural integrity. The design variables include not only the thickness of various components but also parameters that influence structural geometry, such as the width of spar caps, which require a complete remeshing process. As described in Section 2. based on the set of design variables, the wing-box FEM is generated using the in-house FUROR code. Subsequently, aeroelastostatic (Nastran sol 144 [13]) and buckling (Nastran sol 105 [13]) analyses are performed to ensure structural integrity.

Specific constraints are imposed for composite materials, particularly using a first-ply failure approach and considering both Hoffman and maximum strain failure theories. The parameters for the composite CFRP material used for the wing box are reported in Table 20.

Property	Value	Unit
Young's Modulus 1	122.45	GPa
Young's Modulus 2	8.07	GPa
Poisson's Ratio 12	0.321	-
Shear Modulus 12	3.79	GPa
Density	1480.0	kg/m³
Tensile Strength 1 (Ultimate)	866.67	MPa
Compressive Strength 1 (Ultimate)	479.87	MPa
Tensile Strength 2 (Ultimate)	20.51	MPa
Compressive Strength 2 (Ultimate)	97.56	MPa
Shear Strength 12 (Ultimate)	68.12	MPa
Maximum Strain 1 (Ultimate)	2000	microstrain

Table 20 – CFRP uniaxial ply properties from [18]. Ultimate strengths are shown with a safety factor of 0.5 applied. Direction 1 corresponds to the fiber direction, and direction 2 corresponds to the perpendicular direction.

To drive the optimization process, an open-source implementation of NSGA-II [19] is utilized, with consideration for discrete design variables. To achieve a more realistic design and reduce computational time, all DVs are discretized. The discretization steps for each DV are detailed in Table 21; for example, the ply thickness is discretized with a step size of 0.05 mm to align with practical manufacturing constraints. Design variables are defined at the root, kink, and tip sections, then the thickness is linearly interpolated for each bay. A quasi-isotropic and symmetric lamination is considered for the spar web and the skin, where only the thickness of the 0° plies is treated as Design Variables (DVs). Equal thicknesses are imposed on the 45° , -45° , and 90° plies following a lamination setup of $[0^{\circ},45^{\circ},-45^{\circ},90_{2}^{\circ},-45^{\circ},45^{\circ},0^{\circ}]$. For the ribs, the same lamination setup is used, but the ply thickness is fixed at 0.6 mm. An unidirectional ply is considered for the spar cap, and its thickness is treated as a Design Variable. The number of stringers is fixed at 9 for the first section up to the kink, and at 4 for the second section. Only the stringer section height is defined as design variables; these are assumed to be hat-type sections with a thickness equal to 10% of the height, lower base width 20% of the height, and upper base width 80% of the height.

For the sake brevity, Table 21 presents the initial guesses and optimized design variables, while Figure 5 illustrates the objectives and constraints specific to the PEMFC+BAT configuration during optimization. Similar trends were observed in the other configurations and are therefore not detailed here. Following this, the section proceeds to compare all three configurations.

As shown in Figure 5, the optimizer achieves a significant reduction in wing-box mass compared to the initial guess. Among the structural constraints, the maximum ply fiberwise strain is the most critical (considering CFRP properties detailed in Table 20). Conversely, for the PEMFC+BAT configuration, the constraints related to the maximum ply failure index, determined by the Hoffman failure theory, and the buckling load factor are not active.

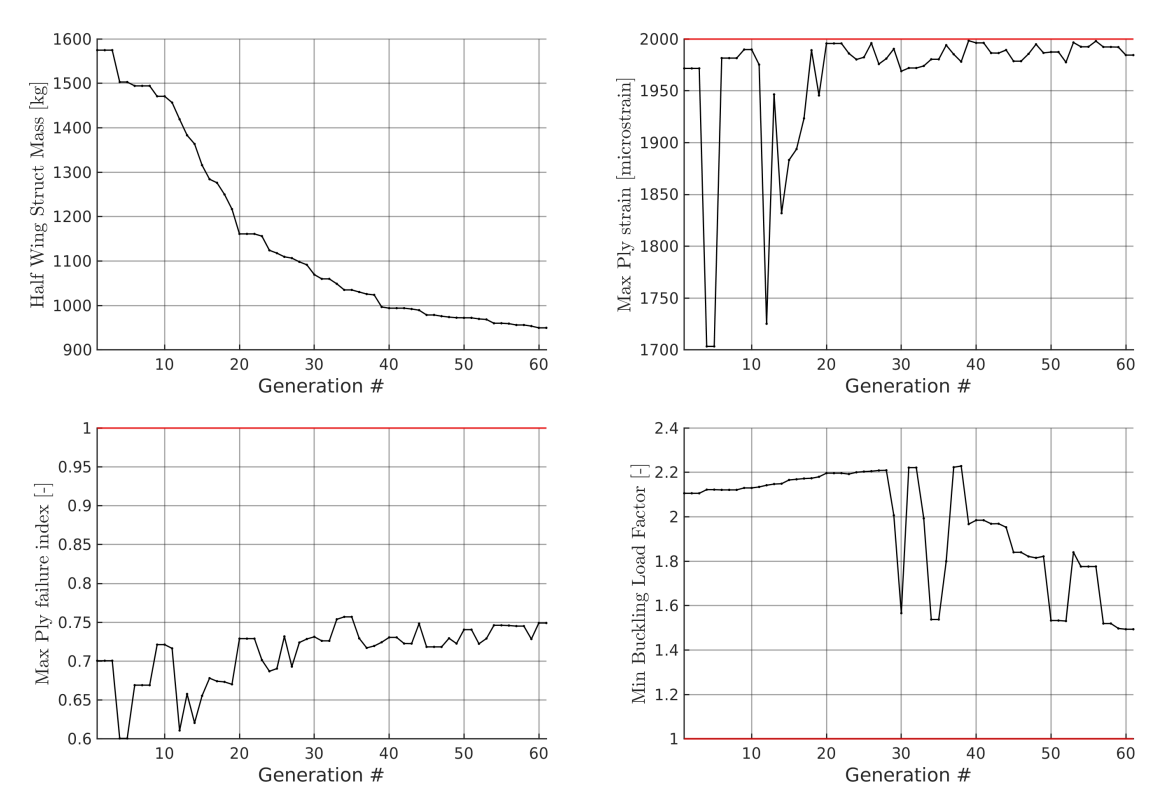


Figure 5 – Objective function and constraints across iterations (generations) of the genetic optimization algorithm for the PEMFC+BAT wing-box. In red are represented the upper or lower constraint.

To achieve a reduction in wing structural weight while maintaining structural integrity, the optimizer employs significant thickness tapering along the spanwise direction. This is evident in Table 21, which lists the design variable values at the root, kink, and tip, as well as in Figure 6 which illustrates spar caps and skin thicknesses for the optimized configurations. Indeed, for some design variables, the optimizer approaches closely to the lower bounds, such as the stringers dimensions and the spar cap width at the tip (see Table 21).

The influence of tapering is also evident in the stress field and the failure criteria fields (maximum strain and Hoffman) presented in Figure 7. Notably, the failure indices remain relatively uniform until past the kink section. This indicates an optimized lightweight structure where tapering effectively maintains a near-limit, uniform stress distribution across a significant portion of the component, thereby achieving weight savings.

Design Variable	Lower	Upper	Initial	Optimized	Discretization
	Bound	Bound	Guess		Step
Spar Web Thickness Root 0 [mm]	0.20	16.00	4.00	2.40	0.05
Spar Web Thickness Kink 0 [mm]	0.20	6.00	2.00	1.05	0.05
Spar Web Thickness Tip 0 [mm]	0.20	1.60	0.80	0.25	0.05
Spar Cap Width Root [%]	2.0	10.0	5.0	6.8	0.1
Spar Cap Width Kink [%]	2.0	6.0	4.0	4.0	0.1
Spar Cap Width Tip [%]	2.0	4.0	3.0	2.2	0.1
Spar Cap Thickness Root 0 [mm]	1.0	100.00	84.00	87.20	0.1
Spar Cap Thickness Kink 0 [mm]	1.0	100.00	50.00	38.30	0.1
Spar Cap Thickness Tip 0 [mm]	1.0	40.00	40.00	3.20	0.1
Skin Thickness Root 0 [mm]	0.20	11.20	2.80	1.20	0.05
Skin Thickness Kink 0 [mm]	0.20	3.60	1.20	1.05	0.05
Skin Thickness Tip 0 [mm]	0.20	1.60	0.80	0.2	0.05
Stringers Height Root [mm]	20.00	150.00	100.00	38.0	1.00
Stringers Height Kink [mm]	20.00	100.00	60.00	20.0	1.00
Stringers Height Tip [mm]	20.00	60.00	30.00	20.0	1.00

Table 21 – Design variables with their bounds, initial guesses, and discretization steps for the PEMFC+BAT configuration. Spar cap width is expressed as a percentage of the wing-box skin chordwise length.

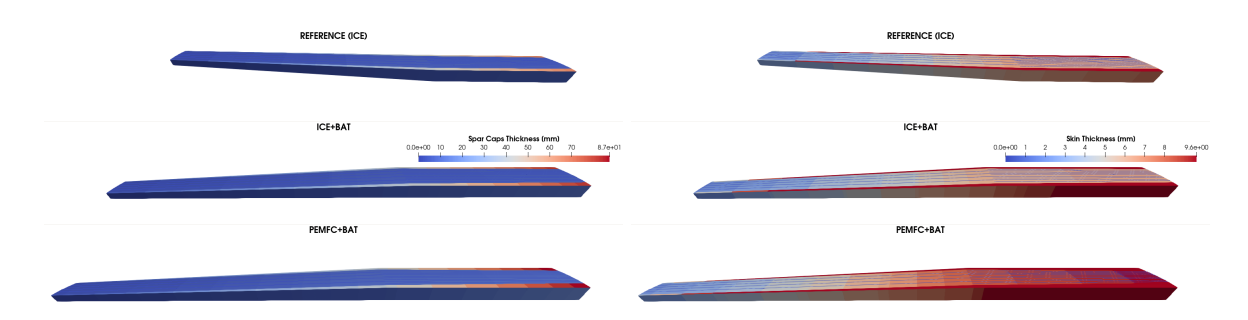


Figure 6 – Optimized spar cap and skin thicknesses for the three configurations.

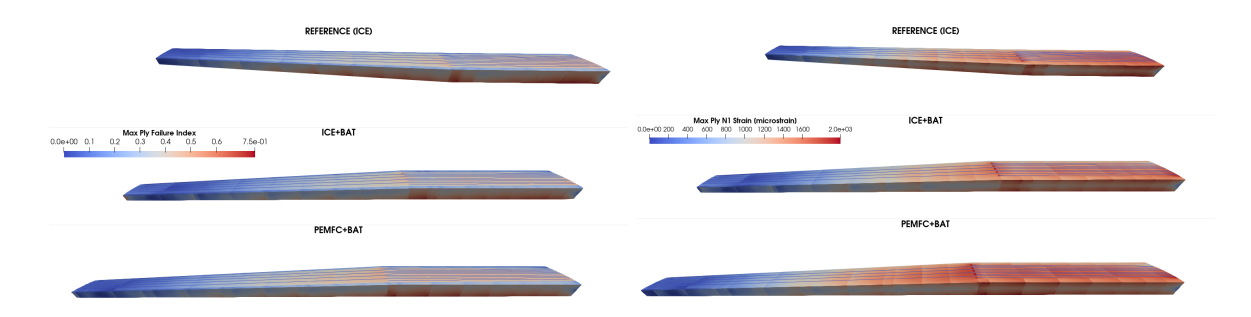


Figure 7 – Optimized maximum ply failure index and maximum ply fiberwise directional strain for the three configurations. The first load case in Table 19 is considered.

Table 22 provides an overview of the structural masses across the three configurations as estimated by both the HEAD empirical relations and the FEM weight estimator. Detailed data for the wing-box includes masses from both the initial guess and the optimized finite element (FE) model. Conversely, for structural components like the fuselage and tail, only initial guess masses are reported. Indeed, these components show notable deviations from the HEAD estimates, with the fuselage exhibiting particularly significant differences. Future efforts will concentrate on optimizing the fuselage structure to address these disparities.

There is a notable correlation between the optimized FEM structural weight of the wing and the

weight estimated by HEAD. However, for the reference ICE and the ICE+BAT configurations (lighter configurations), HEAD overestimates the wing structural weight. Conversely, for the PEMFC+BAT configuration (heavier configuration), HEAD underestimates the weight.

Property	Reference (ICE) [kg]	ICE + BAT [kg]	PEMFC + BAT [kg]
Wing struct. Init. Guess FEM	1549.2	1825.7	3149.8
Wing struct. Optimized FEM	1039.5	1367.1	1899.4
Wing struct. HEAD	1484.0	1580.2	1790.8
Fuselage struct. FEM	3109.6	3120.2	4480.4
Fuselage struct. HEAD	2374.3	2397.5	3183.6
Tail struct. FEM	133.3	124.3	137.6
Tail struct. HEAD	201.0	210.9	241.3
Rudder struct. FEM	243.7	211.7	243.5
Rudder struct. HEAD	257.4	309.3	370.7

Table 22 – Comparison of structural weights across different configurations. The structural masses estimated with HEAD (see Section 4.) are included for comparison. For the wing-box, both the oversized initial guess design and the optimized design structural masses are reported.

5. Conclusions

This study explored the limitations of traditional weight estimation methods (Class I & II) when applied to innovative green aircraft designs, with a particular focus on the wing-box structure. These methods were employed during the conceptual design phase using the in-house HEAD software, which analyzed three distinct aircraft configurations: a reference regional aircraft, a hybrid-electric aircraft, and a full-electric aircraft.

Class I & II methods faced challenges due to their inability to effectively incorporate novel propulsion systems like Distributed Electric Propulsion (DEP) and the unique characteristics of advanced materials such as Carbon Fiber Reinforced Plastic (CFRP).

To address these challenges, a novel Class III weight estimation approach was developed and tested in this study. This approach offers several advantages: it rapidly generates detailed aircraft models using the Finite Element Method (FEM) in under a minute, facilitating swift design iterations and optimization cycles. Unlike traditional methods, Class III includes comprehensive structural analysis capabilities for aeroelasticity and buckling, ensuring robust structural integrity across various flight conditions. Moreover, Class III accurately models composite structures like CFRP, providing more realistic weight estimates compared to traditional methods that often overlook these advanced materials.

The developed Class III approach is implemented across the three aircraft configurations resulting from the conceptual design phase. This approach focuses on optimizing the wing-box structure, incorporating a wide array of design variables such as ply thickness, spar cap width, and stringer dimensions. Additionally, it integrates suitable failure theories for composite materials, including maximum strain and Hoffman criteria. The optimization process employs a genetic algorithm (NSGA-II) to efficiently explore the design space, achieving substantial weight reduction compared to the initial wing-box design while ensuring structural integrity. A key optimization strategy involves tapering the thickness along the spanwise direction of the wing-box, significantly reducing the dimensions of components such as spar caps, skins, and stringers from the wing root to the tip.

The structural masses determined using the Class III approach are compared with those estimated by HEAD. There is a notable correlation between the optimized Finite Element Method (FEM) weight and HEAD's estimates for the wing-box. However, HEAD tends to overestimate the weight for lighter configurations (ICE and ICE+BAT), while underestimating it for the heavier PEMFC+BAT configuration. Larger discrepancies are observed for other structural components like the fuselage and tail, which were not optimized in this study.

Future developments will focus on optimizing the fuselage structure, considering significant concentrated masses specific to green configurations such as batteries or fuel cells. This optimization aims to enhance the accuracy of structural mass estimations across all components of the aircraft.

Acknowledgments

This work is part of the research activity developed by the authors within the framework of the "PNRR" CN4 MOST (Mobilità sostenibile): SPOKE 1 (Air Mobility), WP5: "Multidisciplinary design optimization and innovative solutions for next-generation green aircraft with demonstrator" and SPOKE 1 (Air Mobility), WP4: "Scalable, Safe and Silent next generation aircraft with demonstrator". RMG acknowledges the financial support from the Italian Ministry of University and Research in the framework of the project "National Center for "HPC, Big Data and QC" funded by EU – NextGenerationEU.

6. Contact Author Email Address

mailto: luca.pustina@uniroma1.it

7. Copyright Statement

The authors confirm that they, and/or their company or organization, hold copyright on all of the original material included in this paper. The authors also confirm that they have obtained permission, from the copyright holder of any third party material included in this paper, to publish it as part of their paper. The authors confirm that they give permission, or have obtained permission from the copyright holder of this paper, for the publication and distribution of this paper as part of the ICAS proceedings or as individual off-prints from the proceedings.

References

- [1] N. Thonemann, K. Saavedra-Rubio, E. Pierrat, K. Dudka, M. Bangoura, N. Baumann, C. Bentheimer, P. Caliandro, R. De Breuker, C. De Ruiter, *et al.*, "Prospective life cycle inventory datasets for conventional and hybrid electric aircraft technologies," in *Journal of Cleaner Production*, vol. 434, 2024.
- [2] F. Orefice, P. Della Vecchia, D. Ciliberti, and F. Nicolosi, "Preliminary design to fulfil future market demand of electric aircraft," in *International Review of Aerospace Engineering*, vol. 14, pp. 294–308, 2021.
- [3] V. Marciello, F. Orefice, F. Nicolosi, D. Ciliberti, and P. Della Vecchia, "Design of hybrid-electric aircraft with fault-tolerance considerations," in *Chinese Journal of Aeronautics*, vol. 36, pp. 160–178, 2022.
- [4] E. Torenbeek, "Synthesis of subsonic airplane design: An introduction to the preliminary design, of subsonic general aviation and transport aircraft," in *Delft: Delft University Press*, 1982.
- [5] D. Raymer, *Aircraft design: a conceptual approach*. American Institute of Aeronautics and Astronautics, Inc., 2012.
- [6] J. Roskam, Airplane Design Part I. Lawrence, Kansas: DARcorporation, 1986.
- [7] D. Howe, Aircraft Conceptual Design Synthesis. London: Professional Engineering Publishing, 2000.
- [8] A. Elham, G. La Rocca, and M. J. van Tooren, "Development and implementation of an advanced, design-sensitive method for wing weight estimation," *Aerospace Science and Technology*, vol. 29, no. 1, pp. 100–113, 2013.
- [9] G. Bindolino, G. Ghiringhelli, S. Ricci, and M. Terraneo, "Multilevel structural optimization for preliminary wing-box weight estimation," *Journal of Aircraft*, vol. 47, no. 2, pp. 475–489, 2010.
- [10] M. Sensmeier, B. Stewart, and J. Samareh, "Rapid generation and assessment of aircraft structural topologies for multidisciplinary optimization and weight estimation," in 47th AIAA/ASME/ASCE/AHS/ASC Structures, Structural Dynamics, and Materials Conference 14th AIAA/ASME/AHS Adaptive Structures Conference 7th, p. 1981, 2006.
- [11] L. Pustina, M. Blandino, P. P. Ciottoli, F. Mastroddi, *et al.*, "Towards multidisciplinary design optimization of next-generation green aircraft," in *Towards Multidisciplinary Design Optimization of Next-Generation Green Aircraft*, 2023.
- [12] C. Geuzaine and J.-F. Remacle, "Gmsh: A 3-d finite element mesh generator with built-in pre-and post-processing facilities," *International journal for numerical methods in engineering*, vol. 79, no. 11, pp. 1309–1331, 2009.
- [13] W. P. Rodden and E. H. Johnson, *MSC/NASTRAN aeroelastic analysis: user's guide; Version 68.* MacNeal-Schwendler Corporation, 1994.
- [14] M. S. Corporation, MSC Nastran Quick Reference Guide. MSC Software Corporation, 2021.
- [15] S. Corcione, V. Cusati, V. Memmolo, F. Nicolosi, and R. L. Sandin, "Impact at aircraft level of elastic efficiency of a forward-swept tailplane," in *Aerospace Science and Technology*, vol. 140, 2023.
- [16] A. De Marco, P. M. D'Onza, and S. Manfredi, "A deep reinforcement learning control approach for high-performance aircraft," in *Nonlinear Dynamics*, vol. 111, pp. 17037–17077, 2023.
- [17] G. Di Mauro, S. Corcione, V. Cusati, V. Marciello, M. Guida, and F. Nicolosi, "The potential of structural batteries for commuter aircraft hybridization," in *Journal of Materials Engineering and Performance*, vol. 32, pp. 3871 3880, 2023.
- [18] J. Tomblin, J. McKenna, Y. Ng, and K. S. Raju, "Advanced general aviation transport experiments b basis design allowables for epoxy based prepreg newport graphite unitape g150 nass / nct321 agate-wp3.3-033051-096 july 2001," Technical Report AGATE-WP3.3-033051-096, National Institute for Aviation Research, Wichita State University, Wichita, KS 67260-0093, 2001.
- [19] J. Blank and K. Deb, "pymoo: Multi-objective optimization in python," *IEEE Access*, vol. 8, pp. 89497–89509, 2020.